Materials Today Physics 20 (2021) 100473

Contents lists available at ScienceDirect

Materials Today Physics

journal homepage: https://www.journals.elsevier.com/materials-today-physics

Van der Waals electride: Toward intrinsic two-dimensional ferromagnetism of spin-polarized anionic electrons

Hyun Yong Song [a, b, 1], Byung Il Yoo [a, b, 1], Jin-Ho Choi [c, d, 1], Se-Hwang Kang [a], Joonho Bang [a], Wei Li [c, d], Chandani N. Nandadasa [e], Dinesh Thapa [e], Duhee Yoon [a, b], Myung Joon Han [f], Kyu Hyoung Lee [g], Seong Gon Kim [e, **], Kimoon Lee [h, ***], Sung Wng Kim [a, b, *]

[a] Department of Energy Science, Sungkyunkwan University, Suwon, 16419, Republic of Korea
[b] Center for Integrated Nanostructure Physics, Institute for Basic Science, Suwon, 16419, Republic of Korea
[c] College of Energy, Soochow Institute for Energy and Materials Innovations, Soochow University, Suzhou, 215006, China
[d] Key Laboratory of Advanced Carbon Materials and Wearable Energy Technologies of Jiangsu Province, Soochow University, Suzhou, 215006, China
[e] Department of Physics & Astronomy and Center for Computational Sciences, Mississippi State University, Mississippi State, MS, 39762, USA
[f] Department of Physics, Korea Advanced Institute of Science and Technology (KAIST), Daejeon, 34141, Republic of Korea
[g] Department of Materials Science and Engineering, Yonsei University, Seoul, 03722, Republic of Korea
[h] Department of Physics, Kunsan National University, Gunsan, 54150, Republic of Korea

ARTICLE INFO

Article history:
Received 1 April 2021
Received in revised form
10 June 2021
Accepted 25 June 2021
Available online 30 June 2021

Keywords:
Van der Waals materials
Electrides
Two-dimensional ferromagnetism
Spin-polarized electrons
Anionic electrons

ABSTRACT

Discoveries of two-dimensional (2D) magnetism originated from confined atomic layers in van der Waals (vdW) crystals provide an interesting arena for elucidating its fundamentals and enrich magneto-electric and quantum properties. However, a material that exhibits intrinsic 2D magnetism of interstitial electrons occupying layered space, as a root system of magnetic vdW crystals, remains obscure. In this work, 2D ferromagnetic vdW electride, $[RECl]^{2+}\cdot 2e^{-}$ (RE = Y and La) is reported with perfectly isolated ferromagnetic 2D blocks encompassing quasi-atomic electron layers. The ferromagnetism of the vdW electride with Curie temperature of 100 K originates from the spin-polarized quasi-atomic electrons with a substantial moment up to ~0.91 Bohr magneton, which behave as magnetic elements in paramagnetic lattice framework. Invariable ferromagnetism at the monolayer limit strongly supports the 2D ferromagnetism of quasi-atomic electrons. These findings expand the variety of 2D magnetic crystals, providing a promising platform to study the emergent magnetism of low-dimensional electron phases.

1. Introduction

Two-dimensional (2D) van der Waals (vdW) materials have attracted great interests from recent discoveries of exotic properties such as intrinsic 2D magnetism. Based on their exceptional 2D magnetic properties, 2D magnetic materials with anisotropic vdW bonding have demonstrated the potentials in quantum magneto-electronics and magneto-optics, which can open up a wide range of possibilities for fundamental research and applications for next-generation devices [1–3]. In principle, long-range magnetic ordering can successfully survive overcoming strong thermal fluctuations due to high magnetic anisotropy of 2D layered structure, leading to emergence of an intrinsic 2D ferromagnetism [4–6]. However, the magnetism of 2D vdW crystals is primarily ascribed to the magnetic layers which consist of magnetic constituent elements coordinated with halogens and chalcogens as reported in CrI_3, $Cr_2Ge_2Te_6$, $FePS_3$, and $MnSe_2$ magnets [4,5,7,8]. There also remains a non-negligible interlayer exchange interaction between the magnetic layers crossing a vdW gap due to an insufficient 2D isolation of magnetic layers, providing a layer-dependent magnetism and different bulk magnetic properties from the magnetic monolayer.

Electride, which is an emergent magnetic material of electron

* Corresponding author. Department of Energy Science, Sungkyunkwan University, Suwon, 16419, Republic of Korea.
** Corresponding author.
*** Corresponding author.
E-mail addresses: sk162@msstate.edu (S.G. Kim), kimoon.lee@kunsan.ac.kr (K. Lee), kimsungwng@skku.edu (S.W. Kim).
[1] These authors contributed equally to this work.

https://doi.org/10.1016/j.mtphys.2021.100473

itself, has been of interest due to its exotic characteristic feature that anionic electrons occupying interstitial cavity space in positively charged lattice framework have a noticeable spin moment [9–14]. In early organic electrides with cavity-trapped anionic electrons, a connecting channel along one direction allows the antiferromagnetic coupling between adjacent electrons [9]. It is also reported that the strong localization of anionic electrons in potassium electride under high-pressure induces a Stoner-type instability, leading to the ferromagnetism [10]. A notable fact is that the constituent elements in cationic lattice frameworks of those electrides are all paramagnetic, implying that the anionic electrons are responsible for the emergence of magnetism. From the rigorous studies on diverse 2D electrides, it has been addressed that the exceptional magnetic properties are associated with localization degree of interstitial anionic electrons (IAEs) at the 2D interlayer spaces [11–14]. The 2D $[Ca_2N]^+\cdot e^-$ electride with fully delocalized 2D electron layer showed no magnetic property [11], while the 2D $[Y_2C]^{2+}\cdot 2e^-$ and $[Gd_2C]^{2+}\cdot 2e^-$ electrides with strongly localized electrons at specific crystallographic sites showed the superparamagnetism and ferromagnetism, respectively [12,14]. In particular, for ferromagnetic $[Gd_2C]^{2+}\cdot 2e^-$, it is predicted that the strongly localized IAEs act as quasi-atoms having substantial magnetic moments as ferromagnetic elements in typical magnetic materials [14]. Motivated from the orbital-free nature of these spin-polarized quasi-atomic IAEs under 2D topology, we anticipate that 2D electrides can be a promising candidate for realizing intrinsic 2D magnetism overcoming interlayer magnetic interactions and limited combination of typical magnetic constituent elements. However, the ever-reported 2D electrides are constructed by the ionic bonding between cationic layer units and quasi-atomic IAEs at interlayer spaces, hindering 2D magnetism due to lack of long-range order in spite of highly anisotropic feature (Fig. 1a and b) [11,12,14,15].

We have conceived a different layered structure from previous 2D ionic electrides, which is constructed by the vdW bonding of neutral layers (Fig. 1c), having a potential to realize an intrinsic 2D magnetism based on the quasi-atomic IAEs in 2D electrides. While all the previous 2D ionic electrides are constructed by ionic bonding of IAEs with constituent elements of positively charged layers at interlayer, a 2D vdW electride consists of IAE trapped neutral layers, which are weakly bonded each other by vdW forces. In the structure of 2D vdW electride, the IAE layers are encompassed in positively charged layer framework, preserving the neutrality of layer unit and the IAEs are strongly localized at specific crystallographic sites as quasi-atoms in the intralayer space. Furthermore, non-magnetic constituent elements are prerequisite to study the 2D magnetism induced by the spin-polarized quasi-atomic IAEs in 2D vdW electride. In this context, we here report the first experimental demonstration of 2D vdW electride of rare-earth monochloride, $[RECl]^{2+}\cdot 2e^-$ (RE = Y and La), which is only composed of non-magnetic RE and Cl elements [16,17]. It has been reported that the RECl compounds can be a promising candidate for the 2D electride with a possible ferromagnetism [18]. From our rigorous experimental and theoretical study, it is clearly verified that the $[RECl]^{2+}\cdot 2e^-$ electrides have 2D vdW structure with a ferromagnetism originating from the spin-polarized quasi-atomic IAEs in the intralayer of 2D space. Most of all, the ferromagnetism of quasi-atomic IAE layers retains down to the monolayer limit, suggesting an intrinsic 2D ferromagnetism of electron itself.

2. Results and discussion

Fig. 1c shows the layered crystal structure of rare-earth monochloride, RECl (RE = Y and La), in which the layered structure consists of edge-sharing octahedral RE_6 units. From the single-crystal X-ray diffraction (XRD) patterns (Fig. 1d and e) and atomic structure observations (Fig. 1f and g), we defined the crystal structure and bonding nature of RECl electride. The XRD patterns of RECl single crystals exhibit the exclusive reflection peaks from the (00l) planes (Fig. 1d and e), confirming the high quality c-axis oriented crystals and ensuring the simple cleaving by a 3 M tape exfoliation (Upper side photos in Fig. 1d and e). The chemical stoichiometry of RE:Cl is quantified as 1:1 for both YCl and LaCl as listed in Table S1, Supplementary data. The calculated surface energies (Fig. S1, Supplementary data) clearly indicate that the termination is preferred at the interlayer between Cl–Cl (8 meV/Å^2) rather than the intralayer between RE–RE (89 and 67 meV/Å^2 for YCl and LaCl, respectively). It is noted that the surface energy range at Cl–Cl interlayer corresponds to the nature of weak vdW bonding [19,20]. This feature in crystal structure is also confirmed by scanning transmission electron microscopy (STEM) observations. It directly displays the hexagonal symmetry of RECl layers with the longer Cl–Cl distance (3.67 Å and 3.66 Å for YCl and LaCl, respectively) than the typical Cl–Cl bonding length [21,22]. Therefore, the layered RECl is classified as a 2D vdW material with weak interlayer interaction via vdW forces between Cl atomic layers.

To experimentally clarify the details of bonding nature in 2D vdW RECl, we analyzed the chemical states by X-ray photoelectron spectroscopy (XPS) measurement as well as Bader charge analysis (Fig. 2a–d and Table 1). As shown from Fig. 2a and b, the major peaks of Y 3$d_{3/2}$ (158.9 eV) and La 4$d_{3/2}$ (103.6 eV) are almost similar to those of rare-earth trichlorides ($RECl_3$) [22]. Comparing with the Bader charge amount between RECl and $RECl_3$ (Table 1 and Table S4, Supplementary data), it can be concluded that RE ions in RECl are trivalent with similar oxidation numbers of RE in $RECl_3$. On the other hand, the Cl 2$p_{3/2}$ were detected at slightly higher binding energies (200.4 and 200.5 eV for YCl and LaCl) compared to those (199 eV and 198.8 eV, respectively) of monovalent Cl^- from YCl_3 and $LaCl_3$ (Fig. 2c and d) [22]. This implies that Cl anions of both YCl and LaCl are in an electron-poor state (approximately $Cl^{0.8-}$) compared to the monovalent Cl^- of typical chloride compounds as observed from other 2D vdW chlorides [23,24]. These results indicate that the layer units of RECl should be positively charged as $[RE^{3+}Cl^{(1-\delta)-}]^{(2+\delta)+}$ (δ ~0.2), allowing the existence of excess anionic electrons of $(2+\delta)e^-$ to ensure the charge neutrality as an electride system.

Electrical properties of the 2D vdW $[RECl]^{2+}\cdot 2e^-$ electrides were successfully measured by employing the stamp method as depicted in Fig. 3a [11]. Temperature (T) dependence of electrical resistivity (ρ) along the in-plane direction (Fig. 3b) indicates that both electrides show a metallic conduction behavior. The $[YCl]^{2+}\cdot 2e^-$ electride exhibits larger ρ and residual resistivity ratio (RRR) compared to those of the $[LaCl]^{2+}\cdot 2e^-$ electride [25], suggesting that the electron-phonon interaction degree in $[YCl]^{2+}\cdot 2e^-$ could be stronger than that in $[LaCl]^{2+}\cdot 2e^-$. Magnetoresistance (MR) for both vdW electrides (Fig. 3c and d) shows a distinct anisotropic behavior depending on the direction of the applied magnetic field (H) as observed in other 2D vdW systems [26,27]. At 2 K, out-of-plane MR of $[YCl]^{2+}\cdot 2e^-$ decreases as H increases, while that of $[LaCl]^{2+}\cdot 2e^-$ shows an upturn when $\mu_0 H$ exceeds 1.7×10^4 Oe. As the negative MR behavior in d-band metal compounds generally originates from s–d interaction [28,29], the s–d interaction is more prominent in $[YCl]^{2+}\cdot 2e^-$ than $[LaCl]^{2+}\cdot 2e^-$, surpassing the Lorentz effect [30] that leads to the positive MR as shown in $[YCl]^{2+}\cdot 2e^-$. Because Y has more localized 3d-orbital than La with 4d-orbital, a larger RRR as well as a stronger negative MR behavior in $[YCl]^{2+}\cdot 2e^-$ can be ascribed to the stronger s–d interaction.

Remarkably, in the T dependence of magnetization (M) and magnetic susceptibility (χ) of both vdW electrides (Fig. 3e and f), the magnetic transition clearly appears near 100 K in the out-of-

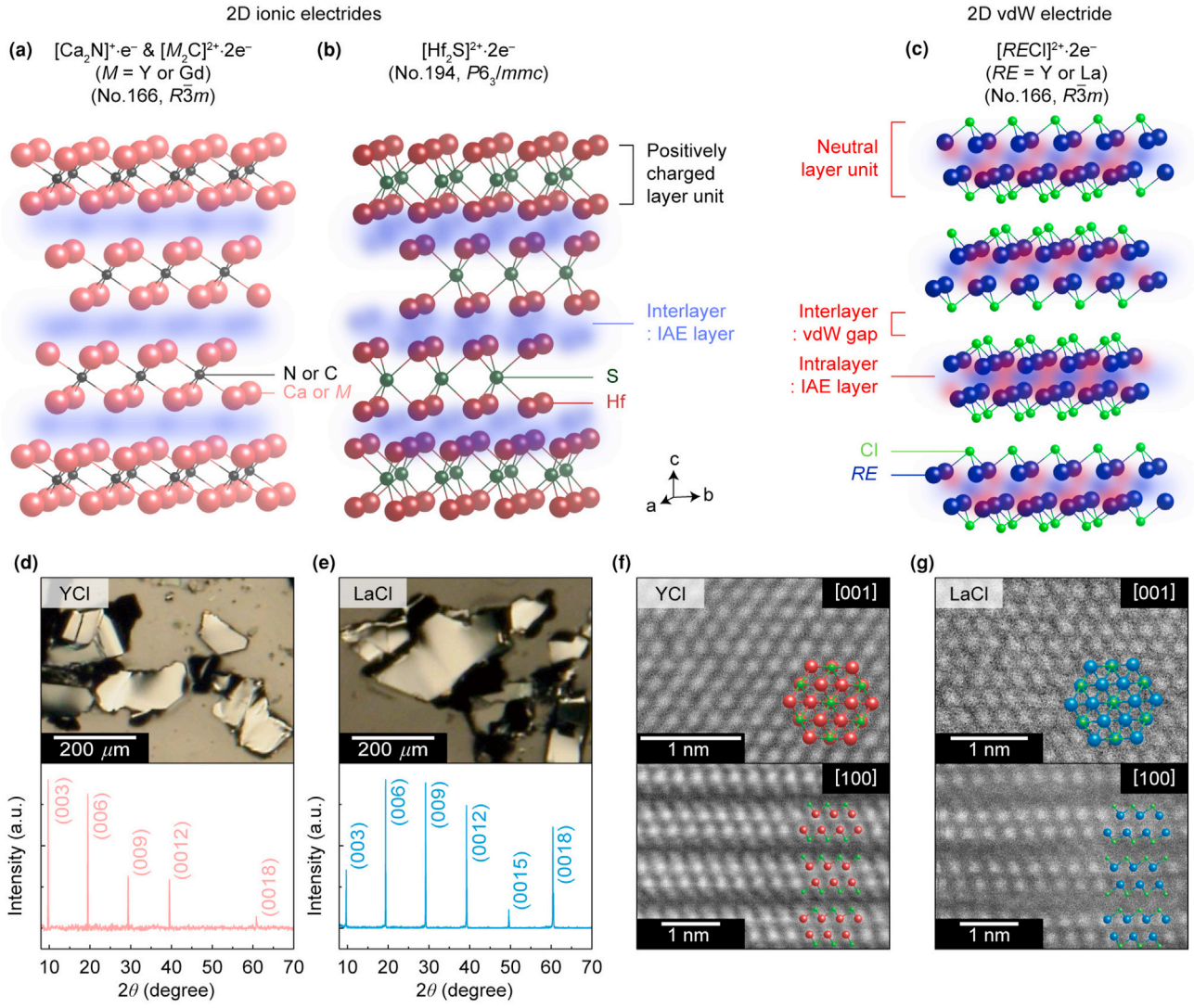

Fig. 1. Van der Waals *RE*Cl electrides. (a, b) Schematic illustration for the crystal structure of previous 2D ionic electrides, $[Ca_2N]^+ \cdot e^-$ and $[M_2C]^{2+} \cdot 2e^-$ (M = Y or Gd) (a) and $[Hf_2S]^{2+} \cdot 2e^-$ (b). (c) Schematic illustration for the crystal structure of *RE*Cl electrides with IAEs in intralayers of *RE*Cl, belonging to the $R\bar{3}m$ space group. Strongly localized IAEs are isolated inside *RE*Cl layer units and each layer is separated by the Cl–Cl vdW interlayer. (d, e) XRD patterns of exfoliated single-crystalline YCl (d) and LaCl (e) electrides. 2θ scan for out-of-plane shows well-oriented reflection in (00l) direction of single-crystalline *RE*Cl electrides. Upper side shows a photograph of exfoliated surface for each *RE*Cl electride. (f, g) Atomic-scale high-angle annular dark field (HAADF)-STEM images along [100] and [001] zone axis of YCl (f) and LaCl electrides (g). STEM results directly prove sufficient Cl–Cl interlayer distance for *RE*Cl electrides to be classified as 2D vdW materials.

plane direction, while a negligible transition is observed in the in-plane direction (see Fig. S3 in the Supplementary data). Fig. 3g and h shows the magnetization (M) of the out-of-plane direction as a function of applied field H at 2 K. Both electrides exhibit nearly saturated moment with negligible hysteresis. It should be noted that the magnetic moments ($\mu_{eff.}$) from the saturated magnetization obtained in M–H curves at 2 K were 0.77 and 0.91μ_B for $[YCl]^{2+} \cdot 2e^-$ and $[LaCl]^{2+} \cdot 2e^-$ electrides, respectively. These ferromagnetic transition and magnitude of moments are unusual when considering that the non-magnetic RE^{3+}, which has no unpaired electrons in d-orbitals, and halogen ions are constituent components of the positively charged lattice framework (See Fig. S4, Tables S2 and S3 in the Supplementary data, that shows a negligible contribution from magnetic impurities). Thus, it is expected that the anionic electrons at the intralayer are responsible for the unusual magnetic properties of $[RECl]^{2+} \cdot 2e^-$ electrides, having a noticeable magnetic moment. Moreover, the experimental result that a higher magnetization value is obtained in the $[LaCl]^{2+} \cdot 2e^-$ electride suggests a more substantial contribution of magnetic anionic electrons in the $[LaCl]^{2+} \cdot 2e^-$ electride. It is noted that the observed magnetic transition is not related to the structural phase transition, as confirmed by the temperature dependent Raman spectroscopy (See Fig. S5 in the Supplementary data).

In order to verify the critical role of magnetic anionic electrons on the unconventional magnetism in $[RECl]^{2+} \cdot 2e^-$ electrides, we conducted *ab initio* calculations based on spin-polarized density functional theory (DFT). A considerable splitting of up (red) and down (blue) spins near E_F distinctly appears as shown in the electronic band structures and density-of-states (DOS) for both electrides (Fig. 4a–d). This ferromagnetic ground state agrees well with the experimental results of magnetic properties. A notable result in the electronic structure is that a significant contribution to the total DOS at the E_F comes from the anionic electrons, not from the constituent *RE* elements (Fig. 4c and d). This major contribution of IAE-projected DOS (IAE-PDOS) at the E_F is the hallmark of an electride [11,12,14]. Compared to the previous 2D electrides, the

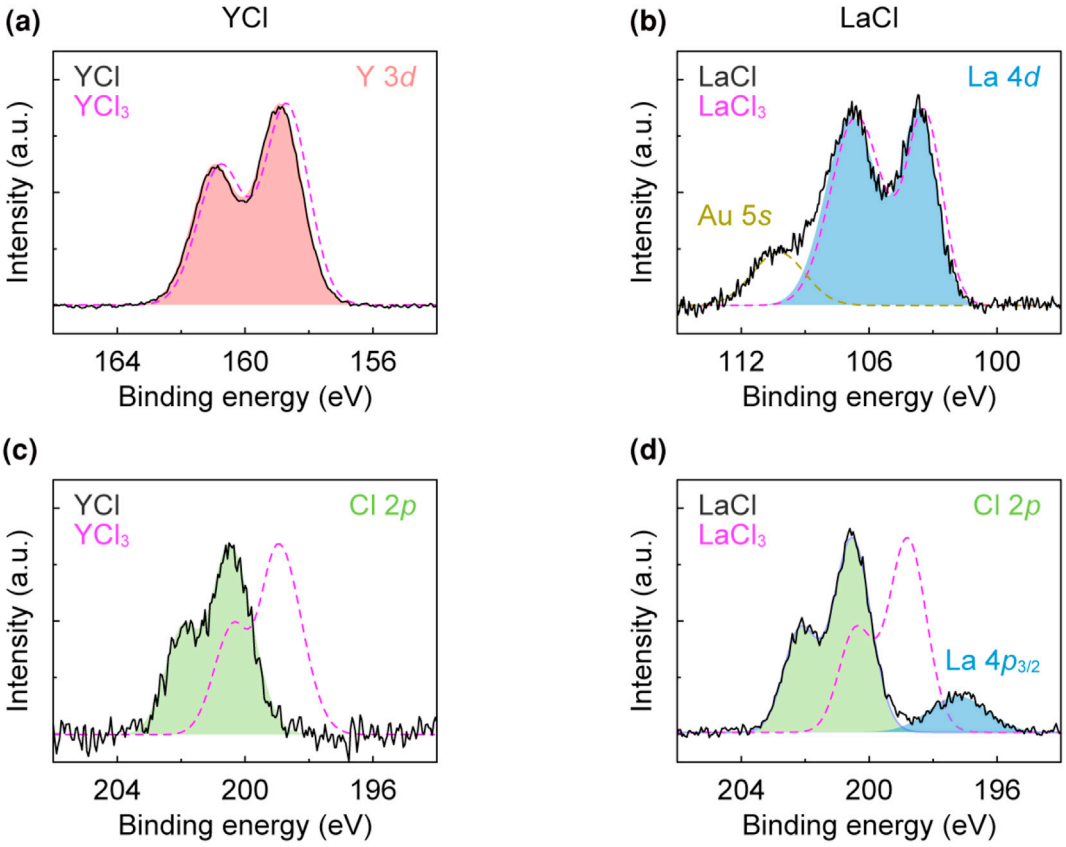

Fig. 2. Chemical states of *RE*Cl electrides. (a–d) XPS spectra of *RE*Cl electrides under the ultra-high-vacuum condition compared with $RECl_3$. The red colored peaks indicate 3*d* of yttrium (a) in YCl electride. The blue colored peaks indicate 4*d* of lanthanum (b) in LaCl electride. The green colored peaks indicate 2*p* of chlorine in YCl (c) and LaCl electrides (d). Binding energy of Y 3*d* and La 4*d* of *RE*Cl show trivalent states similar with those of $RECl_3$. Binding energy of Cl 2*p* of *RE*Cl electrides shows substantial deviation, compare to Cl 2*p* of $RECl_3$. It intimates existence of additional negative charges separated from orbital nature inside lattice framework through the formation of IAEs.

Table 1
Bader analysis for the computational electron counts and local magnetic moments of bulk and monolayer of *RE*Cl electrides.

YCl	Bulk			Monolayer		
Element	(x, x, x)	Oxidation state	Local magnetic moment [μ_B]	(x, x, x)	Oxidation state	Local magnetic moment [μ_B]
Y	x = 0.217	+2.399	0.182	x = 0.217	+2.442	0.206
	x = 0.783	+2.380	0.182	x = 0.783	+2.368	0.205
Cl	x = 0.387	−0.911	0.011	x = 0.387	−0.816	0.016
	x = 0.613	−0.729	0.011	x = 0.613	−0.802	0.016
IAE_A	x = 0.133	−1.207	0.570	x = 0.133	−1.291	0.561
	x = 0.867	−1.232	0.570	x = 0.867	−1.246	0.561
IAE_B	x = 0.500	−0.700	0.000	x = 0.500	−0.652	0.000
	Net magnetic moment [μ_B/f.u.]		0.763	Net magnetic moment [μ_B/f.u.]		0.782
LaCl	Bulk			Monolayer		
Element	(x, x, x)	Oxidation state	Local magnetic moment [μ_B]	(x, x, x)	Oxidation state	Local magnetic moment [μ_B]
La	x = 0.220	+2.255	0.208	x = 0.220	+2.288	0.212
	x = 0.780	+2.226	0.208	x = 0.780	+2.221	0.212
Cl	x = 0.384	−0.873	0.017	x = 0.384	−0.790	0.019
	x = 0.616	−0.706	0.017	x = 0.616	−0.778	0.019
IAE_A	x = 0.126	−1.013	0.664	x = 0.126	−1.085	0.681
	x = 0.874	−1.043	0.663	x = 0.874	−1.051	0.681
IAE_B	x = 0.500	−0.846	−0.001	x = 0.500	−0.801	−0.004
	Net magnetic moment [μ_B/f.u.]		0.888	Net magnetic moment [μ_B/f.u.]		0.909

present vdW electrides are unique in terms of electronic band structure such as dispersion degree of IAE band and its hybridization degree with bands of neighboring cationic elements. Indeed, the band dispersion of IAEs is similar to that of the $[Ca_2N]^+ \cdot e^-$ electride with the largely dispersed band originating from the highly delocalized anionic electron layer [11]. However, in contrast to the $[Y_2C]^{2+} \cdot 2e^-$ and $[Gd_2C]^{2+} \cdot 2e^-$ electrides with a strong hybridization between Y/Gd and IAE bands, a negligible hybridization

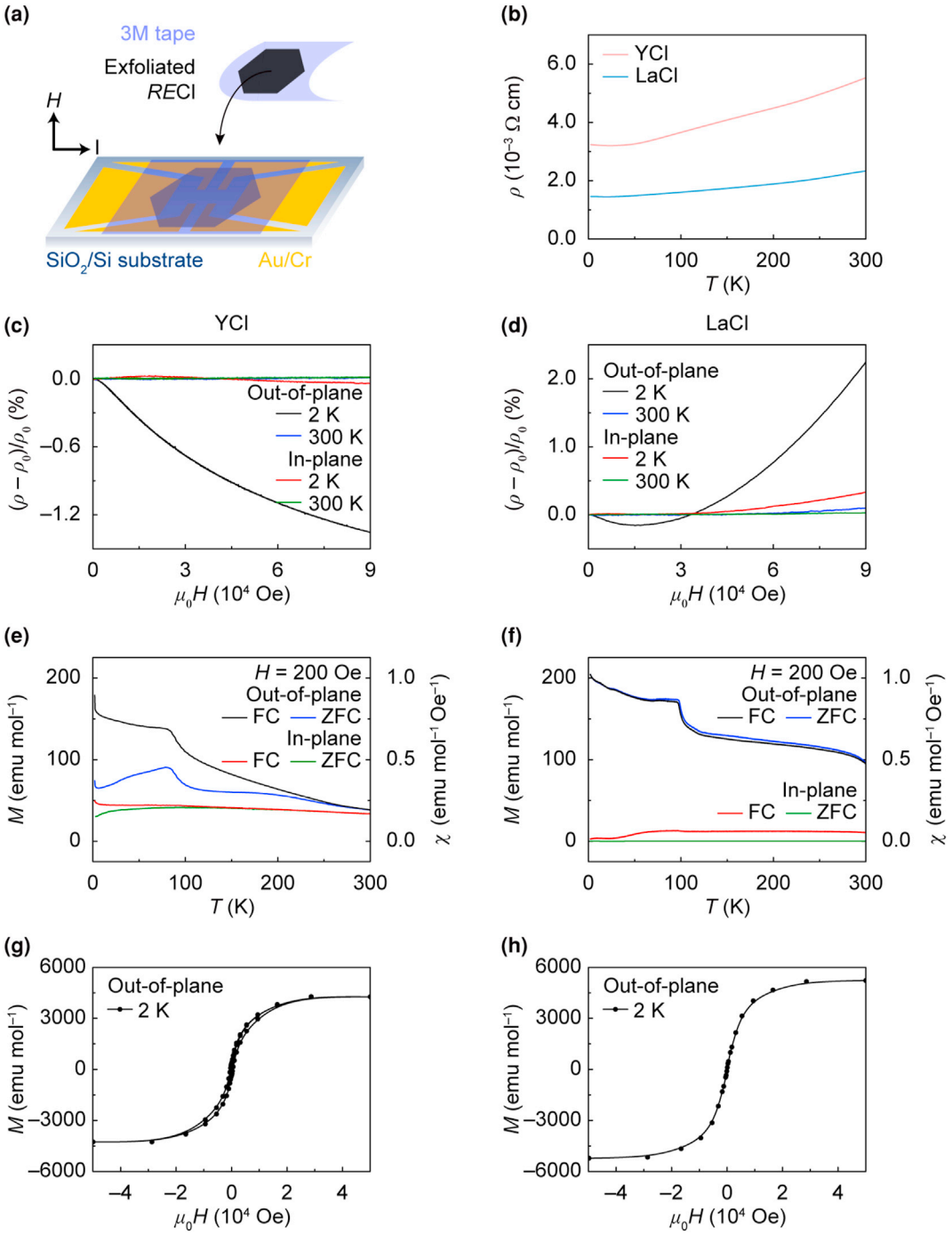

Fig. 3. Electrical and magnetic properties of *RE*Cl electrides. (a) Schematic illustration of measurement for single-crystal flakes of *RE*Cl electride by the stamp method. (b) Temperature (T) dependence of in-plane electrical resistivity (ρ) for single-crystalline *RE*Cl electrides. (c, d) Magnetic field (H) dependence of resistance for YCl (c) and LaCl electrides (d) in different magnetic field directions. (e, f) T dependence of magnetization (M) and magnetic susceptibility (χ) for YCl (e) and LaCl electrides (f) under the 200 Oe of external field with different magnetic field direction. (g, h) M–H curves for YCl (g) and LaCl electrides (h) at 2 K.

between IAE and *RE* bands in $[RECl]^{2+}\cdot 2e^-$ electrides makes a distinct peculiarity [12,14].

In the mapping of electron localization function (ELF), the highly concentrated ELFs in the space between *RE* cations, which are clearly separated from the ELFs of neighboring *RE* cations, appears at two non-atomic positions (Fig. 4e–h). These two positions, IAE_A (black solid circle, A site) and IAE_B (black dashed circle, B site), are defined to have a periodicity as they occupy their own crystallographic Wyckoff sites (Table 1). Thus, the layer units in $[RECl]^{2+}\cdot 2e^-$ electrides are neutralized by the presence of IAEs, having ionic bonding with *RE*–Cl cationic slabs. The most noticeable feature is the different spin state at each IAE site, showing up and down spins for IAE_A and IAE_B, respectively. These spin-polarized IAE_A and IAE_B are responsible for the band splitting at near E_F and the observed magnetic properties. By integrating the charge density within the Bader's basin containing IAEs (Table 1), we obtained the charge of $1.57e^-$ and $1.45e^-$ for $[YCl]^{2+}\cdot 2e^-$ and $[LaCl]^{2+}\cdot 2e^-$, respectively, validating the concept of quasi-atoms for spin-polarized IAEs

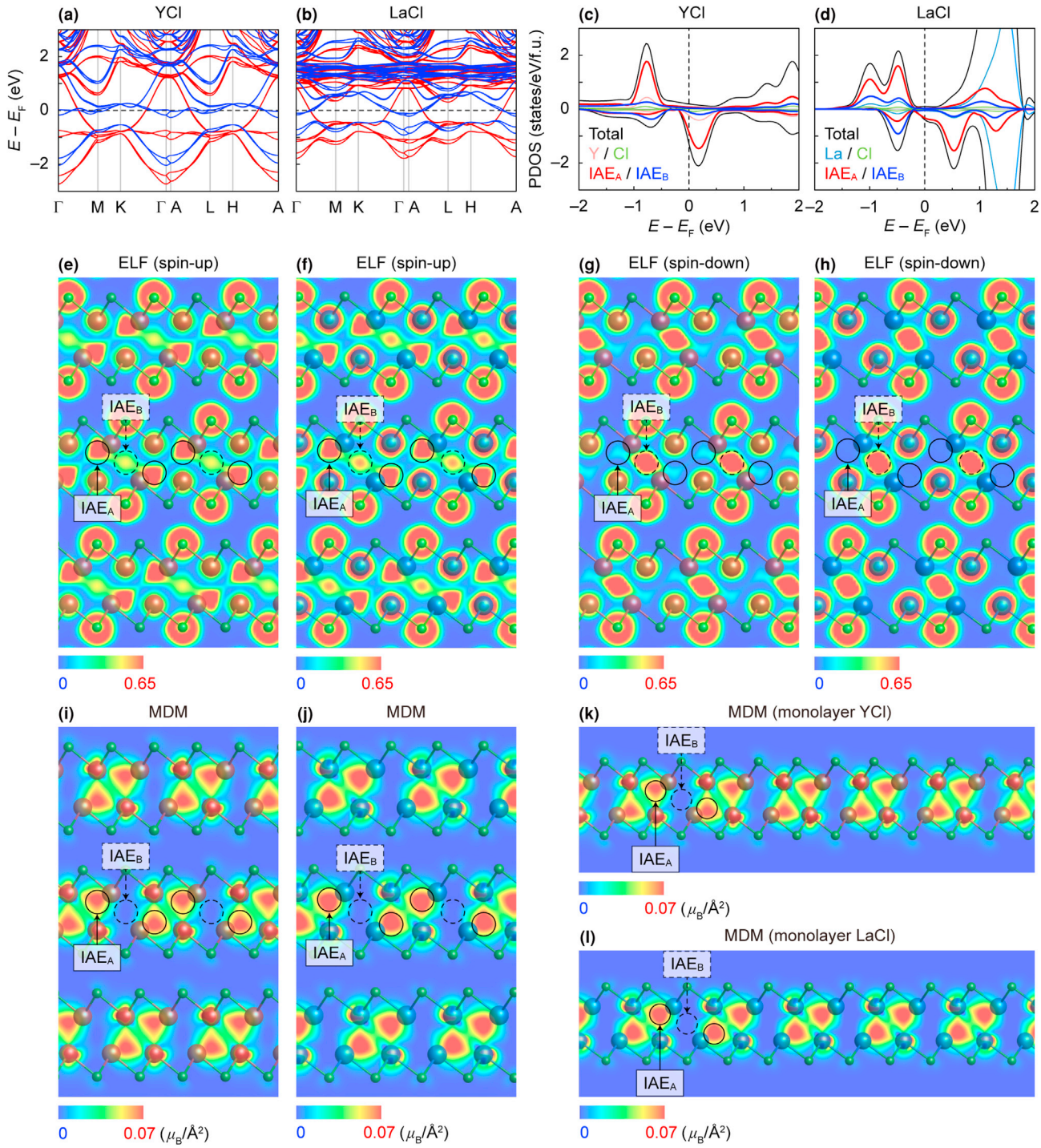

Fig. 4. Ferromagnetism from the spin-polarized quasi-atomic IAEs in vdW *RE*Cl electrides. (a, b) Calculated spin-polarized band structures of bulk YCl (a) and LaCl electrides (b) (spin-up: red color, spin-down: blue color). (c, d) Calculated results of total and projected DOS of bulk YCl (c) and LaCl electrides (d). (e, f) ELF of spin-up state for bulk YCl (e) and LaCl electrides (f) on the (110) plane. (g, h) ELF of spin-down state for bulk YCl (g) and LaCl electrides (h) on the (110) plane. (i, j) MDM of bulk YCl (i) and LaCl electrides (j). (k, l) MDM of monolayer YCl (k) and LaCl electrides (l).

[31,32]. Therefore, it is concluded that the experimentally observed ferromagnetism in the present vdW electrides originates from the spin-polarized quasi-atomic IAEs at intralayer space, not from the orbital electrons of constituent elements.

The magnetic density maps (MDMs) of both electrides show a clear picture of the magnetism originating from the spin-polarized quasi-atomic IAEs (Fig. 4i and j). The position of maxima in MDMs emerges at the site of spin-up IAE, indicating that the quasi-atomic IAE_A has a substantial magnetic moment, while no magnetic density appears at IAE_B site. The local magnetic moments for each IAE and constituent elements are quantified by Bader analysis as listed in Table 1, revealing that the ferromagnetism of both electrides is mainly ascribed to the quasi-atomic IAE_A in the 2D electron layer. In spite of the short distance between IAE_A and *RE* (2.17 Å and 2.35 Å

for $[YCl]^{2+}\cdot 2e^-$ and $[LaCl]^{2+}\cdot 2e^-$, respectively), there is a rare sharing of ELF. On the other hand, a significant sharing of ELF between IAE_A–IAE_B is observed, suggesting that the magnetic exchange integral, which should be critically related to the degree of overlap of the interacting orbitals, is much more significant between IAE_A–IAE_B than IAE_A–*RE*. From the fact that the indirect exchange between non-neighboring magnetic ions can be mediated by a non-magnetic ion [33,34], such a superexchange interaction possibly plays a key role in promoting the spin-alignment of IAEs. Wan et al. also predicted YCl as an electride exhibiting non-zero magnetic moment based on DFT calculation, but they interpreted that ELF at B site can only be considered as the IAE, and the magnetism possibly originates from the exceptionally unfilled *d*-band electrons associated to π-bonding resulting in ELF at A sites [18]. However, our XPS results (Fig. 2) combined with Bader analysis (Table 1, and Table S4 in Supplementary data) definitely confirm that both Y and La are trivalent ions without unfilled *d*-band electron, thus it can be concluded that the experimentally observed ferromagnetism from our layered vdW chlorides originates not from conventional orbital electrons but from the spin-polarized IAEs especially at A sites. Additionally, we examined the critical role of spin-polarized IAEs for the occurrence of ferromagnetism by calculating the PDOS of hydrogen-incorporated *RE*Cl compounds in the chemical formula of $REClH_{1.0}$ and $REClH_{1.5}$ (Fig. S6 in the Supplementary data). It is clear that the removal of spin-polarized IAEs induces the magnetic transition from the ferromagnetism to paramagnetism, indicating that the spin-polarized IAEs are responsible for the observed ferromagnetism. This gives an important insight on the present ferromagnetism, which occurs by the magnetic interactions of IAEs in the intralayer of the completely isolated layer units, thus resulting in a strong magnetic anisotropy and classifying the vdW electrides as an intrinsic 2D magnet.

To prove the 2D ferromagnetism of vdW $[RECl]^{2+}\cdot 2e^-$ electrides, we calculated the band structure, PDOS, ELF, and MDM of the monolayers of $[RECl]^{2+}\cdot 2e^-$. As shown in Fig. S7 in the Supplementary data, the spin splitting of electronic band structure, dominant contribution of IAE-PDOS at E_F and quasi-atomic feature of IAEs in the ELF are identical to the bulk $[RECl]^{2+}\cdot 2e^-$ electride, demonstrating the ferromagnetic ground state of $[RECl]^{2+}\cdot 2e^-$ monolayer. Moreover, in the MDM (Fig. 4k,l) plots of the monolayers of $[RECl]^{2+}\cdot 2e^-$, the strongly localized quasi-atomic nature of spin-polarized IAEs is invariant as found in the bulk $[RECl]^{2+}\cdot 2e^-$ electrides. We calculated the net magnetic moments of each monolayer for $[YCl]^{2+}\cdot 2e^-$ and $[LaCl]^{2+}\cdot 2e^-$, and obtained 0.77 and 0.91 μ_B/f.u., respectively, which are almost consistent with the measured and calculated values of bulk $[RECl]^{2+}\cdot 2e^-$. All the consistency strongly indicates that the 2D ferromagnetism of $[RECl]^{2+}\cdot 2e^-$ electrides is not frustrated down to the 2D limit, proving the intrinsic 2D ferromagnetism of vdW electrides.

3. Conclusion

In conclusion, we have discovered the unprecedented 2D vdW $[RECl]^{2+}\cdot 2e^-$ electrides that contain strongly localized quasi-atomic IAEs at the intralayer space, exhibiting ferromagnetic spin polarization. From rigorous experimental and theoretical characterizations, the highly anisotropic behaviors in electrical transport and ferromagnetic properties arise from spin-polarized IAE_A that is mediated by superexchange interaction bridging non-magnetic IAE_B. We have also confirmed that the ferromagnetic layer unit can be perfectly isolated down to monolayer limit, retaining the ferromagnetic ground state. The present discovery of 2D vdW $[RECl]^{2+}\cdot 2e^-$ electride crystals provides an experimental opportunity for studying the fundamentals of magnetic electron layers as well as for fabricating heterostructure-based magneto-optic or magneto-electronic devices with other 2D vdW crystals.

4. Material and methods

Synthesis of RECl electrides crystals: All synthesis and sample preparations were conducted in a purified glovebox filled with high purity Ar gas (99.999%) to prevent the degradation of raw materials and *RE*Cl electrides in ambient atmosphere containing oxygen and water molecules. For YCl electride, 1:1 ratio of Y metal and YCl_3 powders were mixed and pulverized. Then, pelletized mixture was sealed in fused silica tube (12 mm of inner diameter and 16 mm of outer diameter) with high purity Ar gas (99.999%) atmosphere (~1 bar). Sealed fused silica tube was heated at 550 °C for 48 h. The annealed sample was pulverized and pelletized again, followed by wrapping with molybdenum foil. After sealing in fused silica tube (12 mm of inner diameter and 16 mm of outer diameter) with high purity Ar gas (99.999%) atmosphere (~1 bar), the second heating process was conducted at 850 °C for 72 h. Then, the single-crystalline YCl electride in a form of thin flake was finally obtained. For LaCl electride, stoichiometric 2:1 ratio of La metal and $LaCl_3$ powders were mixed, pulverized and pelletized. The pelletized mixture was fully covered with molybdenum foil. Then, the pellet was sealed in fused silica tube under vacuum condition (~10^{-5} mbar). The sealed fused silica tube was heated at 800 °C for 72 h. Then, the single crystalline LaCl electride in a form of thin flake was obtained without the second heating step required for the single crystal growth of YCl electride.

Structural analysis: The crystal structures of *RE*Cl electrides were analyzed by X-ray diffractometry (SmartLab, Rigaku) and Cs-corrected field emission-transmission electron microscopy (JEM-ARM200F, JEOL). For preventing oxidation during measurement of XRD, the samples were prepared under high purity Ar gas (99.999%) atmosphere then analyzed using an atmosphere separator for SmartLab. The TEM sample was prepared by dual-beam focused ion-beam (FIB) (AURIGA CrossBeam Workstation, Carl Zeiss) for thinning and attachment to TEM grid. To prevent oxidation of *RE*Cl electrides, single crystals of *RE*Cl electrides were exfoliated and loaded to FIB and TEM under high purity Ar gas (99.999%) atmosphere using glove bag connected to the chamber entrance.

XPS measurements: The single-crystalline *RE*Cl electrides flakes were measured by scanning photoelectron microscopy (SPEM) with a monochromatic accelerated beam (598.6 eV) in Pohang Accelerator Laboratory (PAL). The single-crystalline *RE*Cl electrides were exfoliated by commercial 3M tapes and transferred on 100 nm of Au/Cr coated SiO_2/Si substrates. While loading and unloading process, the exfoliation and transferring were conducted in high purity Ar gas (99.999%) purged glove bag, connected to the chamber entrance. During the measurements, the chamber pressure was maintained under 3.0×10^{-10} mbar. All measured spectroscopy of *RE*Cl electrides was calibrated with the measured binding energy of Au 4*f* level of the substrates.

Characterization of electrical and magnetic property measurements: For measurement of electrical property in out-of-plane direction, the single-crystal flakes of *RE*Cl electrides were exfoliated by commercial 3M tapes and transferred on the manufactured four-point probe geometry substrates with the stamp method [11]. The measurement was conducted by physical property measurement system (PPMS). For magnetic property of single-crystal flakes, *RE*Cl electrides were exfoliated by commercial Kapton tape and trapped by the straw holder. Exfoliated single crystals were measured by magnetic property measurement system (MPMS). The experimental magnetic moments were calculated based on the saturated magnetization (M_S) values at 2 K for each *RE*Cl electrides according

to the below Equation (1).

$$\mu_{\mathrm{eff.}}(\mu_B / \mathrm{f.u.}) = \frac{Ms \times \mathrm{mol\_}W}{9.274 \times 10^{-24} \times 6.022 \times 10^{23}} \times 10^{-3} \quad (1)$$

Measured saturated magnetization: M_S (emu/g)
Molecular weight: mol_W (g/mol)
Bohr magneton: $\mu_B = 9.274 \times 10^{-24}$ J/T
Avogadro constant: $N_A = 6.022 \times 10^{23}$ mol^{-1}
Conversion factor: 1 emu $= 10^{-3}$ J/T

Density functional theory calculations: The first-principles DFT calculations were performed using the projector-augmented wave (PAW) method [35] implemented in Vienna *ab initio* Simulation Package (VASP) [36,37], with the Perdew-Burke-Ernzerhof exchange-correlation functional [38]. All calculations were spin-polarized. For vdW corrections, the optB86b functional [39] was adopted. The *RE*Cl electrides crystals were simulated using $R\bar{3}m$ structure containing six *RE*Cl electrides formula units (Fig. 1c). The calculated equilibrium lattice constants are $a = b = 3.70$ Å and $c = 27.73$ Å for bulk YCl electride and $a = b = 4.03$ Å and $c = 27.88$ Å for bulk LaCl electride. The cutoff energy for the plane-wave basis set is 600 eV. The Brillouin zone was sampled using a gamma centered $8 \times 8 \times 1$ k-point mesh for structural optimization in both the bulk and monolayer. The k-mesh values were increased to $16 \times 16 \times 2$ and $16 \times 16 \times 1$ for bulk and monolayer respectively during self-consistent energy calculations. The total energy was converged until its value was changing less than 10^{-6} eV between subsequent iterations and all atomic positions and lattice vectors in bulks were allowed to fully relax until the atomic forces are less than 0.001 eV/Å. In the case of monolayer, the vacuum size of ~20 Å was used to safely avoid the spurious interactions among images of the slab due to periodic boundary conditions. The local magnetic moment of each ion including the IAEs was computed by extending Bader's charge decomposition method [40] to magnetization densities that can attain negative values. The Bader volume for each site is computed as the volume containing a single magnetization density maximum and is separated from other volumes by a zero-flux surface of the gradients of the magnitude of the magnetization density.

Credit author statement

Hyun Yong Song: Methodology, Validation, Formal analysis, Investigation, Writing – original draft, Writing – review & editing, Visualization. **Byung Il Yoo:** Methodology, Validation, Formal analysis, Investigation, Writing – original draft, Writing – review & editing, Visualization. **Jin-Ho Choi:** Methodology, Validation, Formal analysis, Investigation, Writing – original draft, Writing – review & editing, Visualization. **Se-Hwang Kang:** Validation, Data curation. **Joonho Bang:** Validation, Data curation. **Wei Li:** Validation, Formal analysis, Investigation. **Chandani N. Nandadasa:** Validation, Formal analysis, Investigation. **Dinesh Thapa:** Validation, Formal analysis, Investigation. **Duhee Yoon:** Validation, Formal analysis, Investigation. **Myung Joon Han:** Validation, Supervision. **Kyu Hyoung Lee:** Validation, Supervision. **Seong Gon Kim:** Methodology, Validation, Formal analysis, Investigation, Resources, Data curation, Writing – review & editing, Supervision, Project administration. **Kimoon Lee:** Methodology, Validation, Data curation, Writing – review & editing, Supervision, Project administration. **Sung Wng Kim:** Conceptualization, Methodology, Validation, Data curation, Writing – review & editing, Supervision, Project administration, Funding acquisition.

Data availability

The authors declare that the main data supporting the findings of this study we contained within the paper. All other relevant data are available from the corresponding author upon reasonable request.

Declaration of competing interest

The authors declare that they have no known competing financial interests or personal relationships that could have appeared to influence the work reported in this paper.

Acknowledgements

This work was supported by the National Research Foundation of Korea (NRF) grant funded by the Korea government (Ministry of Science, ICT & Future Planning) (No.2015M3D1A1070639) and Institute for Basic Science (IBS-R011-D1).

Appendix A. Supplementary data

Supplementary data to this article can be found online at https://doi.org/10.1016/j.mtphys.2021.100473.

References

[1] Z. Wang, I. Gutiérrez-Lezama, N. Ubrig, M. Kroner, M. Gibertini, T. Taniguchi, K. Watanabe, A. Imamoğlu, E. Giannini, A.F. Morpurgo, Very large tunneling magnetoresistance in layered magnetic semiconductor CrI_3, Nat. Commun. 9 (2018) 2516.
[2] K.L. Seyler, D. Zhong, D.R. Klein, S. Gao, X. Zhang, B. Huang, E. Navarro-Moratalla, L. Yang, D.H. Cobden, M.A. McGuire, W. Yao, D. Xiao, P. Jarillo-Herrero, X. Xu, Ligand-field helical luminescence in a 2D ferromagnetic insulator, Nat. Phys. 14 (2018) 277–281.
[3] P. Jiang, L. Li, Z. Liao, Y.X. Zhao, Z. Zhong, Spin direction-controlled electronic band structure in two-dimensional ferromagnetic CrI_3, Nano Lett. 18 (2018) 3844–3849.
[4] B. Huang, G. Clark, E. Navarro-Moratalla, D.R. Klein, R. Cheng, K.L. Seyler, D. Zhong, E. Schmidgall, M.A. McGuire, D.H. Cobden, W. Yao, D. Xiao, P. Jarillo-Herrero, X. Xu, Layer-dependent ferromagnetism in a van der Waals crystal down to the monolayer limit, Nature 546 (2017) 270–273.
[5] C. Gong, L. Li, Z. Li, H. Ji, A. Stern, Y. Xia, T. Cao, W. Bao, C. Wang, Y. Wang, Z.Q. Qiu, R.J. Cava, S.G. Louie, J. Xia, X. Zhang, Discovery of intrinsic ferromagnetism in two-dimensional van der Waals crystals, Nature 546 (2017) 265–269.
[6] Z. Fei, B. Huang, P. Malinowski, W. Wang, T. Song, J. Sanchez, W. Yao, D. Xiao, X. Zhu, A.F. May, W. Wu, D.H. Cobden, J.-H. Chu, X. Xu, Two-dimensional itinerant ferromagnetism in atomically thin Fe_3GeTe_2, Nat. Mater. 17 (2018) 778–782.
[7] J.-U. Lee, S. Lee, J.H. Ryoo, S. Kang, T.Y. Kim, P. Kim, C.-H. Park, J.-G. Park, H. Cheong, Ising-type magnetic ordering in atomically thin $FePS_3$, Nano Lett. 16 (2016) 7433–7438.
[8] D.J. O'Hara, T. Zhu, A.H. Trout, A.S. Ahmed, Y.K. Luo, C.H. Lee, M.R. Brenner, S. Rajan, J.A. Gupta, D.W. McComb, R.K. Kawakami, Room temperature intrinsic ferromagnetism in epitaxial manganese selenide films in the monolayer limit, Nano Lett. 18 (2018) 3125–3131.
[9] J.L. Dye, Electrides: from 1D Heisenberg chains to 2D pseudo-metals, Inorg. Chem. 36 (1997) 3816–3826.
[10] C.J. Pickard, R.J. Needs, Predicted pressure-induced *s*-band ferromagnetism in alkali metals, Phys. Rev. Lett. 107 (2011) 87201.
[11] K. Lee, S.W. Kim, Y. Toda, S. Matsuishi, H. Hosono, Dicalcium nitride as a two-dimensional electride with an anionic electron layer, Nature 494 (2013) 336–340.
[12] J. Park, K. Lee, S.Y. Lee, C.N. Nandadasa, S. Kim, K.H. Lee, Y.H. Lee, H. Hosono, S.-G. Kim, S.W. Kim, Strong localization of anionic electrons at interlayer for electrical and magnetic anisotropy in two-dimensional Y_2C electride, J. Am. Chem. Soc. 139 (2017) 615–618.
[13] J. Park, J.-Y. Hwang, K.H. Lee, S.-G. Kim, K. Lee, S.W. Kim, Tuning the spin-alignment of interstitial electrons in two-dimensional Y_2C electride via chemical pressure, J. Am. Chem. Soc. 139 (2017) 17277–17280.
[14] S.Y. Lee, J.-Y. Hwang, J. Park, C.N. Nandadasa, Y. Kim, J. Bang, K. Lee, K.H. Lee, Y. Zhang, Y. Ma, H. Hosono, Y.H. Lee, S.-G. Kim, S.W. Kim, Ferromagnetic quasi-atomic electrons in two-dimensional electride, Nat. Commun. 11 (2020) 1526.
[15] S.H. Kang, J. Bang, K. Chung, C.N. Nandadasa, G. Han, S. Lee, K.H. Lee, K. Lee, Y. Ma, S.H. Oh, S.-G. Kim, Y.-M. Kim, S.W. Kim, Water- and acid-stable self-

passivated dihafnium sulfide electride and its persistent electrocatalytic reaction, Sci. Adv. 6 (2020): eaba7416.
[16] H. Mattausch, J.B. Hendricks, R. Eger, J.D. Corbett, A. Simon, Reduced halides of yttrium with strong metal-metal bonding: yttrium monochloride, monobromide, sesquichloride, and sesquibromide, Inorg. Chem. 19 (1980) 2128–2132.
[17] R.E. Araujo, J.D. Corbett, Lanthanum monochloride and lanthanum sesquichloride, Inorg. Chem. 20 (1981) 3082–3086.
[18] B. Wan, Y. Lu, Z. Xiao, Y. Muraba, J. Kim, D. Huang, L. Wu, H. Gou, J. Zhang, F. Gao, H. Mao, H. Hosono, Identifying quasi-2D and 1D electrides in yttrium and scandium chlorides via geometrical identification, Npj Comput. Mater. 4 (2018) 77.
[19] J.T. Paul, A.K. Singh, Z. Dong, H. Zhuang, B.C. Revard, B. Rijal, M. Ashton, A. Linscheid, M. Blonsky, D. Gluhovic, J. Guo, R.G. Hennig, Computational methods for 2D materials: discovery, property characterization, and application design, J. Phys. Condens. Matter 29 (2017) 473001.
[20] K. Momeni, Y. Ji, Y. Wang, S. Paul, S. Neshani, D.E. Yilmaz, Y.K. Shin, D. Zhang, J.-W. Jiang, H.S. Park, S. Sinnott, A. van Duin, V. Crespi, L.-Q. Chen, Multiscale computational understanding and growth of 2D materials: a review, Npj Comput. Mater. 6 (2020) 22.
[21] D.E. Williams, L.-Y. Hsu, Transferability of nonbonded Cl··· Cl potential energy function to crystalline chlorine, Acta Crystallogr. Sect. A Found. Crystallogr. 41 (1985) 296–301.
[22] M. Suzuki, T. Yokoyama, M. Ito, Raman spectrum and intermolecular forces of the chlorine crystal, J. Chem. Phys. 50 (1969) 3392–3398.
[23] Y. Uwamino, A. Tsuge, T. Ishizuka, H. Yamatera, X-ray photoelectron spectroscopy of rare earth halides, Bull. Chem. Soc. Jpn. 59 (1986) 2263–2267.
[24] R.L. Daake, J.D. Corbett, Zirconium monobromide, a second double metal sheet structure. Some physical and chemical properties of the metallic zirconium monochloride and monobromide, Inorg. Chem. 16 (1977) 2029–2033.
[25] C. Kittel, P. McEuen, Introduction to Solid State Physics, Wiley, New York, 1996.
[26] H.H. Kim, B. Yang, T. Patel, F. Sfigakis, C. Li, S. Tian, H. Lei, A.W. Tsen, One million percent tunnel magnetoresistance in a magnetic van der Waals heterostructure, Nano Lett. 18 (2018) 4885–4890.
[27] Z. Wang, M. Huang, J. Zhao, C. Chen, H. Huang, X. Wang, P. Liu, J. Wang, J. Xiang, C. Feng, Z. Zhang, X. Cui, Y. Lu, S.A. Yang, B. Xiang, Fermi liquid behavior and colossal magnetoresistance in layered $MoOCl_2$, Phys. Rev. Mater. 4 (2020) 41001.
[28] K. Yosida, Anomalous electrical resistivity and magnetoresistance due to an *s-d* interaction in Cu-Mn alloys, Phys. Rev. 107 (1957) 396–403.
[29] T.-E. Park, B.-C. Min, I. Kim, J.-E. Yang, M.-H. Jo, J. Chang, H.-J. Choi, Exchange-induced electron transport in heavily phosphorus-doped Si nanowires, Nano Lett. 11 (2011) 4730–4735.
[30] C. Kittel, C. Fong, Quantum Theory of Solids, Wiley, New York, 1963.
[31] M.-S. Miao, R. Hoffmann, High pressure electrides: a predictive chemical and physical theory, Acc. Chem. Res. 47 (2014) 1311–1317.
[32] M. Miao, R. Hoffmann, High-pressure electrides: the chemical nature of interstitial quasiatoms, J. Am. Chem. Soc. 137 (2015) 3631–3637.
[33] J.B. Goodenough, Theory of the role of covalence in the perovskite-type manganites [La,M(II)]MnO_3, Phys. Rev. 100 (1955) 564.
[34] Magnetic and dielectric properties, Princ. Inorg. Mater. Des. (2010) 311–376.
[35] P.E. Blöchl, Projector augmented-wave method, Phys. Rev. B 50 (1994) 17953.
[36] G. Kresse, J. Furthmüller, Efficient iterative schemes for ab initio total-energy calculations using a plane-wave basis set, Phys. Rev. B 54 (1996) 11169.
[37] G. Kresse, D. Joubert, From ultrasoft pseudopotentials to the projector augmented-wave method, Phys. Rev. B 59 (1999) 1758.
[38] J.P. Perdew, K. Burke, M. Ernzerhof, Generalized gradient approximation made simple, Phys. Rev. Lett. 77 (1996) 3865.
[39] J. Klimeš, D.R. Bowler, A. Michaelides, Chemical accuracy for the van der Waals density functional, J. Phys. Condens. Matter 22 (2009) 22201.
[40] M. Yu, D.R. Trinkle, Accurate and efficient algorithm for Bader charge integration, J. Chem. Phys. 134 (2011) 64111.